Interaction of spin-polarized atoms with a surface studied by optical-reflection spectroscopy

Stefan Grafström* and Dieter Suter†
Institute of Quantum Electronics, Eidgenössische Technische Hochschule Zürich–Hönggerberg, CH-8093 Zürich, Switzerland
(Received 1 December 1995)

We present an experiment for the investigation of the interaction of spin-polarized Na atoms with a dielectric surface. A laser beam, which is resonant with an atomic transition, probes the spin polarization near the surface. It is reflected at the surface and the change of its polarization is measured. Our analysis takes into account that the spin polarization is reduced near the surface because of surface-induced spin relaxation. The theory shows that strong wall relaxation leads to a clear modification of the shape and strength of the optical line. The dependence of the line shape on the angle of incidence immediately below the critical angle of total internal reflection provides a sensitive tool for the quantitative determination of the depolarization probability ε per wall collision. Measurements performed at a Pyrex glass surface provide a clear experimental confirmation of the theory and yield a value of $\varepsilon \approx 0.5$. The case of weak wall relaxation is exemplified by experimental results from a silicone-coated glass surface, which are equally well reproduced by the theory. The method offers the prospect of using surface-induced spin relaxation for the study of surface properties and atom-surface interactions for various surfaces. [S1050-2947(96)02109-9]

PACS number(s): 34.50.Dy, 32.80.Bx, 32.70.−n

I. INTRODUCTION

The interaction of an atomic vapor with a solid surface may modify the optical properties of the vapor close to the surface. Such effects can be studied by the reflection of a laser beam at the surface. Thereby the atoms in a thin layer, whose thickness is of the order of the optical wavelength, are probed. Information about the atom-surface interaction may be obtained from the characteristic changes of the reflectivity of the interface that occur when the wavelength is scanned across an atomic transition. This technique of reflection spectroscopy—designated as selective reflection or evanescent-wave spectroscopy, depending on the angle of incidence—has been applied in a number of experiments to study alkali-metal atoms close to glass and other dielectric surfaces [1–5]. Deexciting atom-wall collisions lead to a transient behavior of atoms near the surface, which results in a nonlocal response of the atomic medium to the exciting light field and gives rise to sub-Doppler features in the selective-reflection spectra [6–9]. The long-range van der Waals interaction between the atoms and the surface causes a further modification of the spectra [5,10].

Reflection spectroscopy can also be used to investigate the interaction of spin-polarized atoms with a solid surface [11–13]. At the surface the spin polarization is partly destroyed, since atoms colliding with the surface may stay adsorbed for a certain time during which they are subjected to depolarizing local magnetic fields, before they leave the surface again and return to the gas phase. This phenomenon was first encountered in the early experiments on optical pumping in the 1950s and 1960s [14]. The spin relaxation at the walls of the vapor cells represented a serious obstacle in these experiments. It was overcome by the usage of inert buffer gases that slow down the atomic motion thus prolonging the time between wall collisions. Alternatively, certain surface coatings, preferably containing hydrocarbon chains, can be used to prevent relaxation. They exhibit a strongly reduced interaction with the akali-metal atoms as compared with a bare glass surface, mainly due to a smaller adsorption energy, which results in a shorter average dwell time of the atoms on the surface. The weak depolarization at coatings of this kind was studied both theoretically and experimentally in detail mainly by Bouchiat and Brossel who singled out two types of interactions responsible for the depolarization, namely, a dipole-dipole interaction and a spin-orbit interaction [15].

In recent years, investigations of wall-induced depolarization of optically pumped atoms have been resumed in the context of spin-polarized ion sources in nuclear physics [16–19]. In these studies, a main goal was to find surfaces that cause as little depolarization as possible and at the same time meet the requirements of the specific technical application, such as long-term stability. Several experiments that use spin-polarized nuclei to probe glass surfaces [20,21] or crystalline metal surfaces [22] have demonstrated that surface-induced spin relaxation also bears some potential as a tool for studying surfaces and their interaction with atoms in a more general context from the surface-physical point of view. It was shown that relaxation rates provide information about activation energies for desorption and surface diffusion, as well as the local density of states of a metal surface at the Fermi energy. An extension of the studies performed in the 1960s to a wider class of surfaces therefore seems promising.

In most previous experiments on wall relaxation of spin-polarized atoms the decay of the spin orientation was measured in the bulk of the atomic vapor. Under suitable experimental conditions, this decay is predominantly caused by

*Present address: Physikalisches Institut, Universität Heidelberg, Philosophenweg 12, D-69120 Heidelberg, Germany. Electronic address: grafstroem@physi.uni-heidelberg.de
†Present address: Fachbereich Physik, Universität Dortmund D-44221 Dortmund, Germany. Electronic address: Dieter.Suter@physik.uni-dortmund.de

depolarization at the walls of the container and therefore allows one to extract information about the wall relaxation. In contrast to this type of experiment, we have developed a technique, with which the polarization can be measured in the immediate neighborhood of the surface by polarization-selective detection of a reflected laser beam. We described the basic technique together with some theoretical considerations in an earlier paper [12]. The theoretical treatment presented there did not yet take the wall relaxation into account, but assumed a homogeneous spin polarization throughout the atomic medium. However, the experimental data provided some evidence that wall relaxation leads to a characteristic modification of the observed signal. Meanwhile, we have extended the theory to include the influence of wall relaxation, thus opening up the possibility of studying this phenomenon quantitatively by our technique. We presented a brief report on first quantitative results on the depolarization of spin-polarized Na atoms at a bare glass surface in Ref. [13]. The present paper provides the detailed theoretical basis and gives a more complete presentation of experimental results including both bare and coated glass surfaces.

In our experiment the atomic vapor in front of the surface under study is optically pumped with a laser beam of constant power, which produces a ground-state-spin orientation. In the steady state, diffusion of the atoms in a buffer gas, spin relaxation at the surface, and the optical pumping of atoms leaving the surface lead to a gradient of the spin polarization perpendicular to the surface, so the medium becomes optically inhomogeneous. The experimental setup is described in Sec. II. In Sec. III we work out a comprehensive theoretical analysis, taking fully into account the spatial inhomogeneity of the medium caused by wall relaxation. Section IV presents the experimental results and their interpretation on the basis of the theory. Finally, Sec. V summarizes the results and gives an outlook.

II. EXPERIMENTAL SETUP

The system investigated in our experiment consists of spin-polarized Na atoms in Ar buffer gas in the vicinity of a glass surface. The spin polarization in the Na ground state, which is created by optical pumping of the atoms with a circularly polarized pump beam tuned to the Na D_1 line ($\lambda = 590$ nm), manifests itself as a macroscopic magnetization and makes the medium circularly birefringent. The atoms close to the surface are probed by reflection of a linearly polarized probe beam at the glass-vapor interface. The anisotropy of the atomic medium reveals itself through a change of the polarization of the reflected probe beam.

The experimental setup is sketched in Fig. 1. Na vapor together with 130 mbar Ar (as measured at room temperature), serving as a buffer gas, is contained in a heated glass cell that carries a glass prism on one side. The linearly polarized probe beam is delivered by a dye laser and hits the interface between the prism and the atomic vapor at an angle of incidence that can be varied in a small interval (± 10 mrad) around the critical angle of total internal reflection with a resolution of ~ 0.1 mrad. The polarization of the reflected light is analyzed by means of a differential photodetector that measures the intensity difference between two orthogonally polarized components of the light, which are

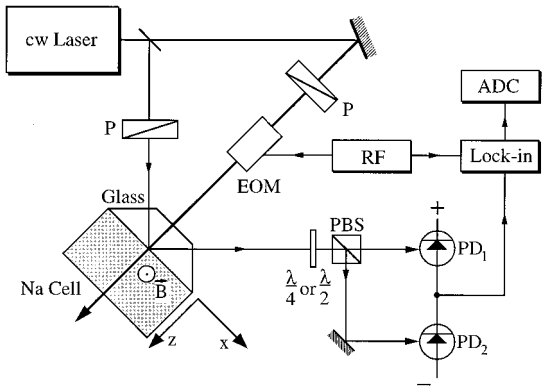

FIG. 1. Experimental setup and definition of the reference frame. P's, polarizers; EOM, electro-optic modulator; RF, frequency synthesizer; ADC, analog-to-digital converter; $\lambda/4$ or $\lambda/2$, retardation plate; PBS, polarizing beam splitter; PD's, photodiodes.

selected by a retardation plate and a polarizing beam splitter. The pump beam is derived from the same dye laser and passed through the glass-vapor interface at normal incidence. A magnetic field is applied perpendicularly to the pump and the probe beam, and an electro-optic modulator modulates the polarization of the pump beam between left and right circular. This results in a forced precession of the magnetization around the magnetic-field direction at the modulation frequency [23]. The modulation frequency is set to the Larmor frequency, which causes a resonant enhancement of the precessing magnetization. The precession gives rise to a modulation of the optical anisotropy and a corresponding modulation of the polarization of the reflected probe beam. Consequently, the signal can be extracted by a lock-in amplifier, which ensures a very high detection sensitivity.

The experiment allows two modes of operation. On one hand, the modulation frequency may be set to the Larmor frequency and kept constant, while the laser frequency is scanned across the optical transition (the D_1 line in our case) and the optical resonance is recorded. On the other hand, we can record the magnetic resonance by tuning the modulation frequency across the Larmor frequency, while keeping the laser frequency constant at or close to the center of the D_1 line. In this paper, we only discuss the optical resonance and always assume that the modulation frequency coincides with the Larmor frequency.

We used two kinds of cells, both made of Pyrex glass. In one cell, we coated the walls with polydimethylsiloxane, whereas the second cell was uncoated. The silicone coating is known to prevent spin relaxation by wall collisions to a large extent [19,24], whereas a bare glass surface causes strong depolarization. Hence, the two surfaces are suitable as model systems, as they represent two rather extreme cases. The preparation of the cells has been described elsewhere [12].

The experiments were performed at a cell temperature of ~ 510–550 K with a Na number density of roughly 10^{16}–10^{17} m^{-3} as estimated from the transmissivity of the sample. At the operating temperature the buffer gas pressure was ~ 220–240 mbar. The pump beam had an intensity of ~ 25–75 mW/cm^2, and the probe beam intensity was ~ 2–4 mW/cm^2. The strength of the magnetic field was set

to $\sim 42\ \mu$T, corresponding to a Larmor frequency of ~ 300 kHz. The earth's magnetic field was compensated by three orthogonal pairs of Helmholtz coils.

III. THEORY

A. Reflection matrix

We consider the interface between a homogeneous isotropic medium (glass) and the spin-polarized Na vapor. We neglect the hyperfine structure and treat the D_1 transition as a transition between two states with angular momentum $J=1/2$. This is a good approximation in our experiment, in which the buffer gas causes a strong pressure broadening that results in a homogenous optical line width of ~ 4 GHz and masks the hyperfine structure. The ground-state polarization can be described by a magnetization vector with the components m_x, m_y, and m_z in the reference frame defined in Fig. 1. Light with a frequency close to the D_1 transition, traveling through the polarized medium, experiences a susceptibility given by [25]

$$\overleftrightarrow{\chi}=\chi_0\begin{bmatrix} 1 & im_z & -im_y \\ -im_z & 1 & im_x \\ im_y & -im_x & 1 \end{bmatrix}, \tag{1}$$

where χ_0 is the optical susceptibility of the corresponding unpolarized isotropic vapor.

The reflection at the interface is described by the reflection matrix that relates the p- and s-polarized components E_{ip} and E_{is} of the incident electric field to their reflected counterparts E_{rp} and E_{rs}

$$\begin{bmatrix} E_{rp} \\ E_{rs} \end{bmatrix}=\begin{bmatrix} r_{pp}^{(0)}+\delta r_{pp} & \delta r_{ps} \\ \delta r_{sp} & r_{ss}^{(0)}+\delta r_{ss} \end{bmatrix}\begin{bmatrix} E_{ip} \\ E_{is} \end{bmatrix}. \tag{2}$$

Here, $r_{pp}^{(0)}$ and $r_{ss}^{(0)}$ are the well-known Fresnel coefficients, which describe the case that the atomic vapor is replaced by vacuum [26]. The quantities δr_{ij} represent the modifications caused by the presence of the vapor. As χ_0 is small ($\chi_0 \sim 10^{-5}$) they can be very well approximated in a first-order expansion in terms of the tensor elements χ_{ij}. To lowest order the electric field in the atomic vapor can be approximated by the field $\vec{E}_t$ with the vapor replaced by vacuum. This field is obtained from the incident wave by multiplying its components with the appropriate Fresnel transmission coefficients. $\vec{E}_t$ induces an electric polarization $\vec{P}=\varepsilon_0\overleftrightarrow{\chi}\vec{E}_t$ in the atomic vapor, which contributes to the reflected field. This contribution determines the first-order corrections δr_{ij} to the reflection matrix. As outlined in Sec. I (see Sec. III C for more details), the magnetization of the Na vapor and hence its tensor of susceptibility depends on the distance z from the interface. Nienhuis, Schuller, and Ducloy calculated the reflected field produced by an arbitrary z-dependent polarization [8]. The evaluation of their result with the polarization given by $\vec{P}(z)=\varepsilon_0\overleftrightarrow{\chi}(z)\vec{E}_t$ with $\overleftrightarrow{\chi}(z)$ according to Eq. (1) yields

$$\delta r_{ij}=\frac{a_{ij}}{2\xi}\left\{p_{ij}(0)+\int_0^\infty e^{i2k_0\xi z}\left(\frac{d}{dz}p_{ij}(z)\right)dz\right\}, \tag{3}$$

TABLE I. Prefactors a_{ij} and quantities p_{ij} for the different elements of the reflection matrix. The elements p_{ij} apply to a spin-polarized atomic vapor described in the $J=1/2\leftrightarrow J'=1/2$ model.

ij	a_{ij}	p_{ij}
pp	$1-(r_{pp}^{(0)})^2$	$\frac{\chi_0}{2\xi}(\xi^2-\eta^2+2i\xi\eta m_y)$
ps	$\{[1-(r_{pp}^{(0)})^2][1-(r_{ss}^{(0)})^2]\}^{1/2}$	$\frac{i\chi_0}{2\xi}(\xi m_z-\eta m_x)$
sp	$\{[1-(r_{pp}^{(0)})^2][1-(r_{ss}^{(0)})^2]\}^{1/2}$	$\frac{i\chi_0}{2\xi}(\xi m_z+\eta m_x)$
ss	$1-(r_{ss}^{(0)})^2$	$-\frac{\chi_0}{2\xi}$

where k_0 is the vacuum wave vector [27]. The elements $p_{ij}(z)$ are listed together with the prefactors a_{ij} in Table I. The quantities η and ξ are the sine and the cosine of the angle of refraction θ_t in the absence of the atomic vapor

$$\eta=n_0\sin\theta_i=\sin\theta_t \quad \xi=\sqrt{1-\eta^2}=\cos\theta_t, \tag{4}$$

where θ_i is the angle of incidence and n_0 the refractive index of the glass. Note that ξ is real when θ_i is below the critical angle of total internal reflection θ_c and imaginary when it is above θ_c, whereas η is always real. The expression in Eq. (3) is valid for all angles of incidence except for a narrow interval around θ_c. The width of the excluded interval is roughly given by $\chi_0(\sim 10^{-5})$, which is well below the divergence of the probe beam. Therefore, this restriction has not much practical importance, as the beam averages over a broader interval.

B. Calculation of the signal

In the experiment, the ground-state polarization is created through optical pumping by a pump-laser beam that propagates in the z direction with a polarization that is modulated between right and left circular. The transverse magnetic field is oriented along the y axis and forces the magnetization into a precession around the y axis. In the steady state the magnetization rotates in the x-z plane at the modulation frequency, so the off-diagonal elements of the reflection matrix show a corresponding oscillation, whereas the diagonal elements are constant in time (cf. Table I).

We specify the probe beam, which in linearly polarized at an angle α with respect to the plane of incidence, by its p- and s-polarized electric-field amplitudes

$$\mathbf{I}=\begin{bmatrix} E_{ip} \\ E_{is} \end{bmatrix}=E_0\begin{bmatrix} \cos\alpha \\ \sin\alpha \end{bmatrix}. \tag{5}$$

We obtain the corresponding vector **R** of the reflected wave by operating the reflection matrix on **I**. (We use boldface to distinguish these vectors from the three-dimensional representation.) As described in Sec. II, this wave is analyzed by polarization-selective detection in the following way: A retardation plate together with a polarizing beam splitter defines a pair of mutually orthogonal polarizations, which in the most general case are elliptic and can be described by two unit vectors

$$\mathbf{e}_1=\begin{bmatrix} \cos\beta \\ e^{i\kappa}\sin\beta \end{bmatrix}, \quad \mathbf{e}_2=\begin{bmatrix} \sin\beta \\ -e^{i\kappa}\cos\beta \end{bmatrix}. \tag{6}$$

TABLE II. Theoretical signal $\Delta I/I_0$ for different experimental configurations, expressed in terms of reflection matrix elements. The labels s, p, and 45° refer to linear polarization perpendicular, parallel, and at 45° with respect to the plane of incidence, respectively, whereas r and l denote right and left circular polarization. See text for the definition of the parameters α, β, and κ.

Incident polarization	Analyzer setting	α	β	κ	$\Delta I_{\mathrm{mod}}/I_0$
p	$\pm 45°$	0°	45°	0°	$\mathrm{Re}\{2r_{pp}^{(0)}\delta r_{sp}^{*}\}$
s	$\pm 45°$	90°	45°	0°	$\mathrm{Re}\{2r_{ss}^{(0)}\delta r_{ps}^{*}\}$
45°	$p-s$	45°	0	0°	$\mathrm{Re}\{r_{pp}^{(0)}\delta r_{ps}^{*}-r_{ss}^{(0)}\delta r_{sp}^{*}\}$
p	$l-r$	0°	45°	90°	$\mathrm{Re}\{2ir_{pp}^{(0)}\delta r_{sp}^{*}\}$
s	$l-r$	90°	45°	90°	$\mathrm{Re}\{-2ir_{ss}^{(0)}\delta r_{ps}^{*}\}$

The projections of $\mathbf{R}$ onto $\mathbf{e}_1$ and $\mathbf{e}_2$ are transformed into p- and s-polarized light, respectively, by the retardation plate. The parameters β and κ depend on its orientation and on the phase difference it produces. The beam splitter separates the two components and directs them onto two photodiodes of the differential detector, which measures the intensity difference given by

$$\Delta I=|\mathbf{e}_1\cdot\mathbf{R}|^2-|\mathbf{e}_2\cdot\mathbf{R}|^2. \tag{7}$$

The signal is extracted by means of a lock-in amplifier, which is referenced to the modulation frequency of the pump beam polarization. Therefore, only those parts of ΔI that contain the modulated components of the magnetization (m_x and m_z) contribute to the measured signal, which becomes

$$\begin{aligned}\frac{\Delta I_{\mathrm{mod}}}{I_0}=&\sin(2\alpha)\cos(2\beta)\mathrm{Re}\{r_{pp}^{(0)}\delta r_{ps}^{*}-r_{ss}^{(0)}\delta r_{sp}^{*}\}\\&+2\sin(2\beta)\mathrm{Re}\{e^{i\kappa}(\cos\alpha)^2 r_{pp}^{(0)}\delta r_{sp}^{*}\\&+e^{-i\kappa}(\sin\alpha)^2 r_{ss}^{(0)}\delta r_{ps}^{*}\},\end{aligned} \tag{8}$$

where all higher-order terms were suppressed and $I_0=E_0^2$ is the total intensity of the incident probe beam. In practice, only some particularly simple combinations of incident polarization and analyzer setting are used, involving linear and circular polarizations, as summarized in Table II. In all cases listed, except the third one, the nonmodulated signal background vanishes, which allows a high amplification and helps minimize the noise. In the third case this is true only in the region of total internal reflection, but the dc signal remains small also for partial transmission as long as the angle of incidence is close enough to the critical angle.

C. Inhomogeneous magnetization

Collisions of the atoms with the surface lead to spin relaxation and reduce the atomic polarization close to the probed interface. Therefore, an inhomogeneous layer exists at the interface, across which the magnetization varies as a function of the distance from the interface. Furthermore, we have to keep in mind that the magnetization undergoes a forced precession. The behavior becomes particularly simple if the modulation frequency is equal to the Larmor frequency. Then the component m_z parallel to the pump beam oscillates in phase with the polarization modulation in the sense that it reaches its extreme values each time the pump beam polarization passes through a state of purely circular polarization. Correspondingly, m_x oscillates with the same amplitude but out of phase by 90°. This holds true independently of the effective strength of the relaxation in the buffer gas and at the surface. In the case that the modulation frequency is off resonance a more complicated situation arises, in which not only the magnitude but also the phase of the precessing magnetization varies with the distance from the wall. In this paper we concentrate on the simplest case of on-resonance modulation.

According to Table I the oscillating off-diagonal elements of the reflection matrix contain a contribution from m_x and a contribution from m_z, which, of course, are 90° phase shifted with respect to each other. We can select either part of the signal by properly setting the phase of the lock-in amplifier. In all measurements presented in Sec. IV the out-of-phase signal (with respect to the polarization modulation) was acquired, which means that m_x was selected. The contribution of m_z provides no additional information. This signal part is strongly suppressed close to the critical angle, as m_z is multiplied by ξ (see Table I).

Under the assumption of on-resonance modulation, it is sufficient to consider the amplitude m of the precessing magnetization. We describe its spatial variation by a real function g, such that

$$m(z)=m_\infty g(z) \quad \text{with} \quad g(z)\underset{z\to\infty}{\to}1, \tag{9}$$

where m_∞ is the magnetization in the bulk of the atomic vapor. The variation of m with z is caused by the interplay of the diffusion of polarized atoms to the wall, where their orientation is partly destroyed, optical pumping at a constant rate, and loss of polarization by collisions with buffer gas atoms, by diffusion of atoms out of the pump beam, or by reabsorption of fluorescence light (radiation trapping). The evolution of m with time at a distance z from the surface is described by

$$\frac{\partial m}{\partial t}=D\frac{\partial^2 m}{\partial z^2}+P(1-m)-\gamma m, \tag{10}$$

where D denotes the diffusion coefficient of Na in the buffer gas, P the optical pump rate, and γ the relaxation rate in the buffer gas. The optical pumping (P) represents a source of polarization and drives the system toward complete polarization ($m=1$), but is counteracted by the relaxation in the buffer gas. The stationary solution of Eq. (10) is given by (cf. Fig. 2)

$$g(z)=\frac{m(z)}{m_\infty}=1-(1-g_0)\exp(-\mu z), \tag{11}$$

with the bulk limit $m_\infty=m(z\to\infty)=P/(P+\gamma)$, the boundary condition $m(0)=m_\infty g_0$, and the inverse decay length $\mu=[(P+\gamma)/D]^{1/2}$. The homogeneous case corresponds to $g_0=1$. The boundary condition is determined by the wall relaxation in the following way: One half of the atoms at the wall are atoms arriving from the volume. They have traveled

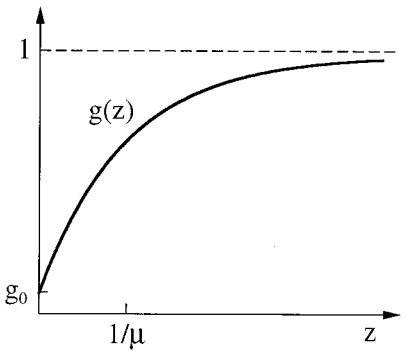

FIG. 2. Normalized magnetization $g=m/m_\infty$ as a function of the distance z from the wall.

a mean distance L in z direction since their last collision with a buffer gas atom, given by 2/3 of the mean-free-path in the buffer gas [28]. Therefore, we assume that their degree of polarization is given by $g(z=L)$. The other half consists of atoms that originally came from the same mean distance carrying the same polarization, but have made a wall collision and return to the gas phase from the surface. These atoms have been partly depolarized, so their polarization is reduced by a factor of $1-\varepsilon$, where ε denotes the probability of depolarization. Within this model g_0 is related to $g(z=L)$ by

$$g_0=\frac{1+(1-\varepsilon)}{2}g(L). \tag{12}$$

This equation in combination with Eq. (11) establishes the following relationship between ε and g_0:

$$\varepsilon=\frac{2\mu L(1-g_0)}{\mu L(1-g_0)+g_0}, \tag{13}$$

where the approximation $\exp(-\mu L)\approx 1-\mu L$ was used, which is valid under typical experimental conditions.

D. Strength and shape of the optical resonance line

As discussed in the preceding subsection, the steady-state magnetization m exhibits a spatial variation close to the wall described by $g(z)$, whereas we assume that the density of the atomic vapor is constant, so χ_0 is constant throughout the medium. In accordance with Eq. (8) and with the proper expressions for δr_{ps} and δr_{sp} [Eq. (3) and Table I] in mind, the signal derived in Sec. III B can now be written as

$$S=\frac{\Delta I_{\mathrm{mod}}}{I_0}=\mathrm{Re}\{m_\infty\chi_0 v\}, \tag{14}$$

where v is a complex-valued function of the angle of incidence of the probe beam and can be expressed as

$$v=v_{\mathrm{hom}}\left\{g(0)+\int_0^\infty e^{i2k_0\xi z}\left(\frac{d}{dz}g(z)\right)dz\right\}, \tag{15}$$

with v_{hom} describing the homogeneous case corresponding to $g(z)=1$ [29]. The expression in braces stems from the evaluation of the reflection matrix. Note that the functional expression for v_{hom} depends on the particular combination of probe beam polarization and analyzer setting. For the explicit form of $g(z)$ given by Eq. (11) the function v becomes

$$v=v_{\mathrm{hom}}g_0\left\{1+\frac{\varepsilon}{2-\varepsilon}\,\frac{1}{\mu L-i2k_0L\xi}\right\}. \tag{16}$$

The dependence of the signal on the laser frequency of the probe beam arises through the susceptibility χ_0, which we assume to be Lorentzian in shape, since the homogeneous pressure broadening caused by the buffer gas in our experiment exceeds the Doppler broadening. With $v=|v|\exp(i\varphi)$, we can rewrite Eq. (14) as

$$S=m_\infty|v|(\mathrm{Re}\{\chi_0\}\cos\varphi-\mathrm{Im}\{\chi_0\}\sin\varphi). \tag{17}$$

Hence, the signal as a function of the laser frequency exhibits a line shape that is a mixing of absorptive ($\mathrm{Im}\{\chi_0\}$) and dispersive ($\mathrm{Re}\{\chi_0\}$) contributions with a mixing angle given by the phase of v. On the other hand, the absolute value $|v|$ characterizes the strength of the signal. In particular, $\varphi=0$ corresponds to a pure dispersion line and $\varphi=-\pi/2$ to a pure absorption line, whereas $\varphi=\pi$ and $\varphi=\pi/2$ give the respective inverted structure.

In an earlier paper, we discussed the case of a homogeneously polarized atomic medium, characterized by $g(z)=1$, for a situation, in which the angle of incidence of the probe beam is close to the critical angle of total internal reflection to within a few mrad [12]. Before we discuss the inhomogeneous case, we summarize very briefly the results of the analysis presented in Ref. [12] for the homogeneous medium, which can also easily be extracted as a special case from the general expressions worked out above: Let $\delta=\theta_i-\theta_c$ be the detuning of the angle of incidence from the critical angle of total internal reflection. For small values of δ, the signal strength given by $|v_{\mathrm{hom}}|$ drops with $1/\sqrt{|\delta|}$ when the angle of incidence is detuned from the critical angle in either direction (actually, this asymptotic behavior is fulfilled better for total reflection than for partial transmission). In all experimental situations summarized in Table II the line shape makes an abrupt transition from purely dispersive to purely absorptive or vice versa at the critical angle, which means that v_{hom} jumps from real to imaginary at this angle.

Let us now turn to the inhomogeneous case. In the region of total internal reflection ξ is purely imaginary and the expression in braces in Eq. (15) becomes real. Therefore, the phase of v does not change compared with the homogeneous case, so the line shape is not affected, but only the strength of the signal is modified. This finding is completely general and does not depend on the specific form of $g(z)$. On the other hand, in the region of partial transmission, where ξ is real, both the line shape and the signal amplitude are modified by $g(z)$.

For a closer discussion of the modifications introduced by the wall relaxation, it is useful first to bring to mind some typical experimental parameters: For an Ar buffer gas pressure $p=230$ mbar and a temperature $T=540$ K the diffusion coefficient D of the Na atoms in the buffer gas is approximately 2 cm^2/s. This follows from the value $D_0=0.2$ cm^2/s listed in Ref. [30] via the transformation $D=D_0(T/T_0)^{3/2}(p_0/p)$ with $T_0=300$ K and $p_0=1013$ mbar. The mean-free-path L_{free} is obtained from D via the relation-

ship $D=L_{\text{free}}\langle v\rangle/3$, where $\langle v\rangle$ denotes the thermal mean velocity [28]. With our parameters we find $L_{\text{free}}\approx 0.9$ μm, and hence $L\approx 0.6$ μm$\approx\lambda$ and $k_0 L\approx 2\pi$. The quantity $P+\gamma$ can be estimated from the width of the magnetic resonance line measured in a bulk experiment [31]. We take $P+\gamma=2\pi\times 10$ kHz as a typical value for the pump beam intensity actually used in the experiment. This gives $1/\mu=56$ μm and $k_0/\mu=600$, which means that the inhomogeneous layer is very thick compared with the optical wavelength. Consequently, even close to the critical angle of total internal reflection, where $|\xi|$ is small, we have $2k_0|\xi|/\mu \gg 1$. For example, $2k_0|\xi|/\mu\geqslant 10$ is fulfilled for $|\delta|$ as small as 0.03 mrad. Hence, Eq. (16) can be approximated by

$$v=v_{\text{hom}}g_0\left(1+\frac{\varepsilon}{2-\varepsilon}\times\frac{i}{2k_0L\xi}\right). \tag{18}$$

Obviously, in the range of partial transmission (ξ real) the phase of v is influenced by the degree of depolarization ε at the surface, so the optical line shape depends on ε. When the angle of incidence approaches the critical angle from the side of partial transmission, ξ is real and goes to zero and the expression in brackets becomes imaginary. Therefore, the phase is shifted by $\pi/2$ as compared with the homogeneous case. However, when the angle of incidence is tuned farther below the critical angle, ξ increases and the bracketed expression approaches 1, so the line shape evolves toward the shape predicted for the homogeneous case.

If we consider as an example a situation where we have a dispersive line shape in the region of total internal reflection, the behavior can be summarized as follows: When the angle of incidence is tuned from above to below the critical angle, the phase makes a jump by π and the line shape is abruptly inverted [actually, the approximate form given by Eq. (18) becomes invalid very close to the critical angle and the inversion is not complete, depending on the value of g_0]. Upon further angular detuning, the line shape then approaches an absorptive shape. How fast this approach occurs strongly depends on the value of ε, which therefore may be determined from a measurement of the line shape as a function of the angular detuning below the critical angle. This will be illustrated by the experimental data discussed in the next section.

IV. EXPERIMENTAL RESULTS AND DISCUSSION

A. Uncoated cell

We first turn to the discussion of the experimental results obtained with the uncoated glass cell, in which a strong surface-induced spin relaxation is expected. The optical line was recorded for a number of different angles of incidence and for several different settings of the analyzer and of the polarization of the probe beam, corresponding to several of the possibilities listed in Table II.

To characterize the line shape and signal strength, we fitted a mixed absorptive-dispersive theoretical line to the experimental data. To achieve a good fit, we must take into account that the pump beam is frequency tuned together with the probe beam. This causes an additional modification of the optical line shape, since the pump rate P varies with the laser frequency. Therefore, the factor $m_\infty g_0$ contained in $S=\text{Re}\{m_\infty\chi_0 v\}$ with v given by Eq. (18), which represents

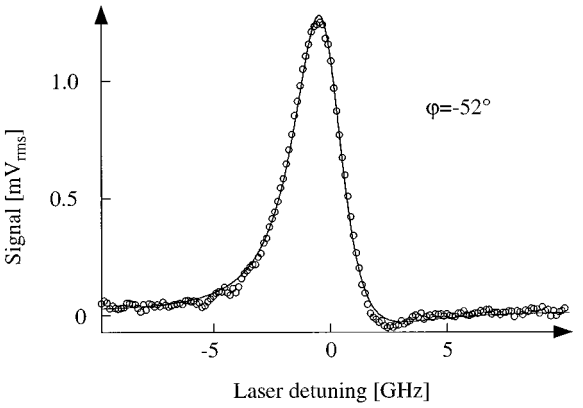

FIG. 3. Signal as a function of the frequency detuning of the laser as measured with the uncoated cell at $\delta=-0.4$ mrad (circles). The theoretical line shape (solid curve) has been fitted to the data. The fit yields a mixing angle $\varphi=-52°$.

the magnetization at $z=0$, is not constant

$$m_\infty g_0=\frac{P}{\sqrt{P+\gamma}}\,\frac{1}{\sqrt{D/L^2}\varepsilon/(2-\varepsilon)+\sqrt{P+\gamma}}. \tag{19}$$

P has an absorptive Lorentzian dependence on the laser frequency detuning, and this leads to an apparent narrowing of the observed line, since the optical pumping becomes less efficient with increasing detuning, so the wings of the line are suppressed. Hence, a purely Lorentzian line does not reproduce the experimental line shape well and a mixed-phase Lorentzian line multiplied by an expression of the type given in Eq. (19) has to be used instead. The damping γ and the pump rate P can be estimated from the dependence of the width of the magnetic resonance line on the pump power [32]. We found $P_{\max}\approx 2\pi\times 10$ kHz for zero laser detuning and $\gamma\approx 2\pi\times 2$ kHz [33]. It follows that in the case of strong wall relaxation (ε close to unity) we have $(D/L^2)^{1/2}\varepsilon/(2-\varepsilon)\gg(P+\gamma)^{1/2}$, so the expression given in Eq. (19) reduces to const $\times P/(P+\gamma)^{1/2}$ and the knowledge of the particular value of ε is not required in advance for the evaluation.

Figure 3 depicts the optical line as measured slightly below the critical angle at $\delta=-0.4$ mrad. The probe beam was s polarized and the intensity difference between the components of the reflected beam polarized at $\pm 45°$ with respect to the plane of incidence was measured. We fitted a theoretical line shape of the type discussed above to the data by adjusting the center frequency, the width, the amplitude, the mixing angle (phase) φ, and a constant background level, while keeping the ratio $P_{\max}/\gamma=5$ fixed in accordance with the above estimation. The experimental line shape is fairly well reproduced by the theoretical curve, but some systematic deviations are nevertheless present (cf. Fig. 3). This is, of course, not surprising with regard to the unresolved hyperfine structure and the Doppler effect, which were both completely neglected in the theory.

To extract the relaxation probability ε, we determined the mixing angle φ as a function of the angular detuning from the critical angle, as depicted in Fig. 4. The theoretical function $\varphi=\arg(v)$, which follows from Eq. (16), was fitted to

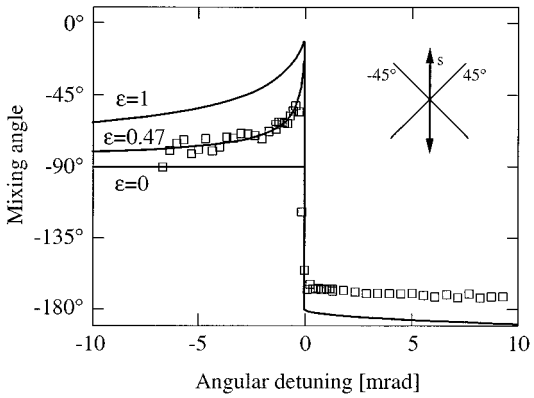

FIG. 4. Mixing angle of the optical line as a function of the angular detuning from the critical angle of total internal reflection. Experimental data (squares) are shown together with theoretical curves for three different values of the depolarization probability. The curve for $\varepsilon=0.47$ represents the best fit to the data.

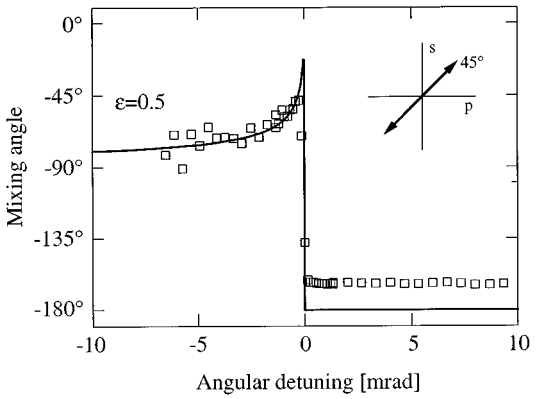

FIG. 5. Mixing angle of the optical line as a function of the angular detuning from the critical angle measured with the probe beam polarization at 45° with respect to the plane of incidence. The intensity difference between the s- and p-polarized components of the reflected beam was detected. The solid curve represents the theoretical behavior for $\varepsilon=0.5$.

the data with ε as the only free parameter and with the assumptions $L=0.6$ μm and $1/\mu=56$ μm. The value of μ influences the curve only in the closest neighborhood of the critical angle, but is of no importance for the overall behavior, which is well described by the approximation given by Eq. (18). Consequently, the value of ε that results from the fit is virtually independent of μ. The fit delivers $\varepsilon=0.47$, corresponding to $g_0=0.034$, and the data are very well described by the theoretical curve in the region of partial transmission.

In the case of total internal reflection the theory predicts the line to be close to an inverted dispersion line independently of the value of ε. This is indeed essentially in agreement with the experiment, although the experimental line shows some asymmetry, which produces a systematic deviation of approximately 15° of the experimental mixing angle from the theoretical values (cf. Fig. 4). A similar asymmetry is observed in an analogous experiment that probes the bulk of the atomic vapor. Here, the probe beam is passed through the vapor cell overlapping with the pump beam and the polarization of the transmitted light is analyzed. The finding that the asymmetry is also present in the bulk suggests that it is not related to the interaction with the surface; we attribute it to the unresolved hyperfine structure.

Note that according to Eq. (18) the quantity that determines the dependence of the line shape on the angular detuning is $k_0L(2-\varepsilon)/\varepsilon$ rather than ε itself. Hence, a possible error of L immediately affects the experimental value of the depolarization probability. Here, both the value of the diffusion coefficient itself as well as its transformation into the mean-free-path L_{free} according to the most simple gas kinetic theory represent possible sources of systematic errors. An additional error may originate from the fact that the description of the basic line shape as Lorentzian is inaccurate because of the hyperfine structure and the Doppler effect. Indeed, we observed that after a slight modification of the functional expression used to describe the line shape the quality of the fit stayed more or less unchanged but the mixing angle provided by the fit nevertheless changed by several degrees. This suggests that the correct theoretical description of the line shape is extremely important in order to achieve reliable results. At present, we estimate the corresponding uncertainty with regard to the depolarization probability to be $\sim 20\%$.

In Fig. 4 the extreme cases of $\varepsilon=0$ and $\varepsilon=1$ are also indicated. It should be stressed that complete depolarization at the wall does not imply that the magnetization at the wall vanishes completely. With the assumptions made about L and μ, we find $g_0=0.01$ for $\varepsilon=1$, which means that the magnetization at the wall is still 1% of the bulk value m_∞, although each wall collision is completely disorienting. This is, of course, due to the magnetization that is carried to the wall from the volume of the atomic vapor. An analogous phenomenon exists when a gas is in contact with a wall that is kept at a different temperature than the volume of the gas itself. Then there is a temperature gradient across a certain layer of the gas close to the wall due to heat conduction, but the temperature of the gas in the immediate neighborhood of the wall is not equal to the temperature of the wall, a phenomenon known as ''surface jump'' [28,34]. The surface jump of the magnetization at a completely disorienting surface in our experiment is determined by the product μL and depends on the buffer gas pressure.

Figure 5 shows the result obtained with the probe beam polarized at 45° with respect to the plane of incidence and with the reflected beam analyzed in terms of its s- and p-polarized components. In the case of partial transmission, the behavior is identical to the one discussed above in full agreement with the theory. Within the statistical error both measurements yield the same depolarization probability ε. For total internal reflection, we again observe a systematic deviation of the same kind as above. However, it is interesting to note that in spite of this offset of the absolute value of the mixing angle φ the experiment follows the theoretical predictions as far as the change of φ with the angular detuning δ is concerned: in Fig. 4 there is a slight decrease of φ with increasing δ, whereas in Fig. 5 φ stays constant. Furthermore, with the configuration of Fig. 4 but with the probe beam p polarized, we observed a slight increase of φ in agreement with the theory (not shown).

Not only the mixing angle φ but also the signal strength

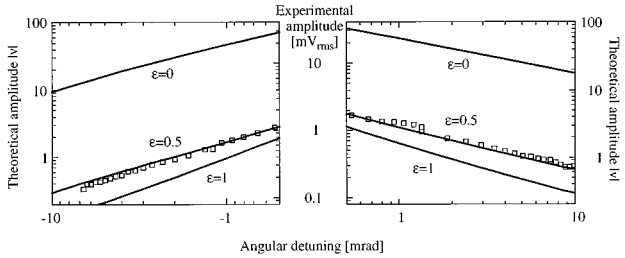

FIG. 6. Signal strength as a function of the angular detuning from the critical angle. The squares indicate the experimental data and the curves represent the theory for three different values of ε. They were calculated for $1/\mu=56$ μm and $L=0.6$ μm. The logarithmic ordinates for theory and experiment have been adjusted with respect to each other to bring theory and experiment into line for $\varepsilon=0.5$.

provides information about the depolarization at the surface. The dependence of the signal strength on the angular detuning is shown in Fig. 6, in which the experimental data are depicted vs the angular detuning δ in two log-log plots (for $\delta<0$ and $\delta>0$, respectively), together with theoretical curves corresponding to $\varepsilon=0$, $\varepsilon=0.5$, and $\varepsilon=1$. The signal always reaches its maximum for zero angular detuning and falls off on both sides of the critical angle (somewhat more rapidly for partial transmission than for total reflection). With increasing ε, this signal decay becomes steeper. In the angular regime depicted in Fig. 6, the dependence can be rather well approximated by a power law $|\delta|^s$ with s between -0.5 and -1 but different for $\delta<0$ and $\delta>0$ and depending on the value of ε. In the absence of wall relaxation ($\varepsilon=0$) the theory predicts $s\approx-0.5$ for total reflection and $s\approx-0.7$ for partial transmission. In the extreme case of total depolarization at the surface the values are closer to -1. Note that according to Eq. (18) the power s, which is the slope of the curve in the log-log plot, is only determined by ε and L but independent of μ. In the approximation represented by Eq. (18) the latter quantity only enters the problem within the prefactor g_0 and therefore only shifts the curves vertically in the log-log plot without changing their shape and slope. Unless the density of the sodium vapor and a number of experimental parameters such as photodiode sensitivities and light powers are accurately known, we cannot evaluate the absolute signal amplitude quantitatively and the comparison between experiment and theory must be restricted to the slope s. The experimental slope is very well reproduced by $\varepsilon=0.5$ in agreement with the result obtained from the evaluation of the line shape (see above). Therefore, the theoretical curves in Fig. 6 were adjusted in amplitude by a common shift along the ordinate in such a way that the curve for $\varepsilon=0.5$ falls onto the experimental data points, but we would like to stress that the slope and not the amplitude is the relevant feature.

From Fig. 6 it becomes evident that, although the slope s in principle reflects the magnitude of ε, its dependence on ε is not very pronounced and far less characteristic than the dependence of the line shape on the angular detuning. Therefore, the line shape provides the better tool for achieving information about the wall relaxation. But it is worthwhile noting that the slope s reflects the strength of the surface-induced spin relaxation on both sides of the critical angle, in contrast to the line shape that contains information about ε only in the range of partial transmission.

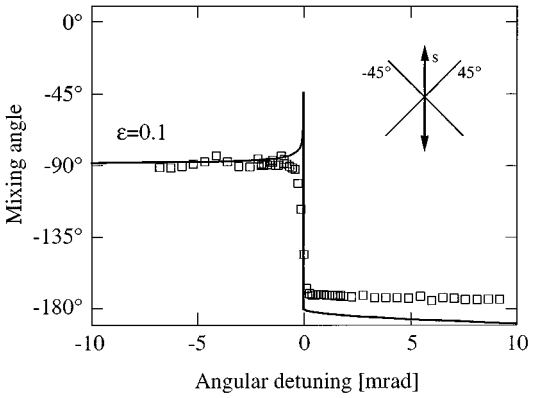

FIG. 7. Mixing angle of the optical line vs angular detuning as measured with a silcone-coated Pyrex glass surface (squares) together with a theoretical curve for $\varepsilon=0.1$. This curve does not represent a fit to the data but serves to illustrate the rather weak dependence of the theoretical mixing angle on ε.

B. Silicone-coated cell

After the detailed presentation of the results from the uncoated glass surface, we now proceed to the discussion of the corresponding data from the silicone-coated surface, for which a much weaker relaxation is expected. Again, the mixing angle and the signal strength were determined for a set of different angles of incidence. This time, the relationship $(D/L^2)^{1/2}\varepsilon/(2-\varepsilon)\gg(P+\gamma)^{1/2}$ does not apply because of the much weaker wall relaxation, and we have to use some presumptive value of ε for the fit. The analysis of the magnetic resonance line indicates that ε is roughly between 0.01 and 0.02 [32]. Taking into account that the pump power was lower than in the previous case, we consider $(D/L^2)^{1/2}\varepsilon/(2-\varepsilon)=P_{\max}^{1/2}$ and $P_{\max}/\gamma=2.5$ to be reasonable assumptions. The small depolarization probability means that the pumping efficiency is now less severely reduced in the wings of the line. As a matter of fact, the line appears wider for the coated than for the uncoated cell as a direct consequence of this effect.

The mixing angle φ, as found from the fit with the parameters chosen as stated above, is depicted in Fig. 7 for the same configuration of probe beam polarization and analyzer setting that was also used in the measurement with the uncoated cell illustrated in Fig. 4. Comparing the two figures, we see that in the region of total internal reflection no significant difference exists. This is indeed exactly the behavior predicted by the theory, according to which the mixing angle is completely independent of the wall relaxation in this angular regime. The systematic deviation of $\sim15°$, which was above tentatively attributed to the hyperfine structure, is present in the coated as well as in the uncoated cell.

Below the critical angle, however, the two cells differ very clearly in their behavior, the line shape observed with the coated surface being almost purely absorptive in the whole region of partial transmission. Along with the experimental data, Fig. 7 shows a theoretical curve for $\varepsilon=0.1$, which differs only little from the curve expected if wall re-

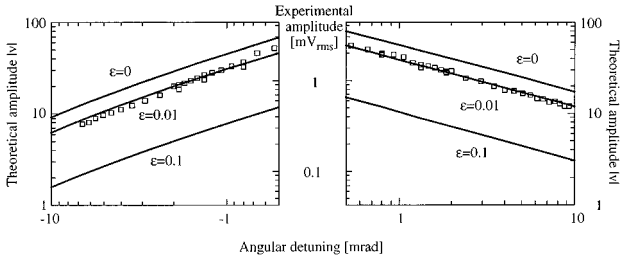

FIG. 8. Signal strength vs angular detuning observed with the coated cell in comparison with theoretical results for three different values of ε between 0 and 0.1.

laxation is completely absent (cf. Fig. 4). Indeed, as far as the mixing angle is concerned, the experiment is compatible with more or less any value of ε between 0 and ~ 0.1, but with values closer to zero appearing somewhat more likely. It is only in the immediate neighborhood of the critical angle where in principle the line shape still shows a more pronounced dependence on ε, but this angular interval is too narrow to be resolved experimentally because of the divergence of the laser beam. One should also keep in mind that the theory becomes inaccurate for very small angular detunings ($|\delta| \sim |\chi_0|$), so they are not well suited for a quantitative evaluation of the data.

It should be pointed out that in contrast to the case of strong wall relaxation the assumptions about the functional form of the line shape do not have very much impact on the mixing angle in the case considered here, as the line is always rather symmetric—either very close to absorptive below the critical angle or close to dispersive above θ_c.

Figure 8 is a log-log plot of the signal amplitude, as acquired with the configuration chosen according to the fifth entry of Table II, together with theoretical curves for $\varepsilon=0$, $\varepsilon=0.01$, and $\varepsilon=0.1$. They have been adjusted arbitrarily to produce the best fit between experiment and theory for $\varepsilon=0.01$. But again it is the slope rather than the absolute amplitude that should attract the reader's attention. From Fig. 8 it becomes obvious that it is not possible to determine ε from the experimental slope. The slopes of all three theoretical curves are in perfect agreement with the experiment within the statistical fluctuations.

In summary, in the case of weak wall relaxation—as represented by the silicone-coated cell—we again find that the theory can well reproduce the experimental data, but a quantitative deduction of ε is not feasible, neither from the line shape nor from the signal strength. It is only possible to put an upper boundary on ε of about 0.1. However, it is worthwhile noting that even a small wall relaxation of $\varepsilon=0.01$ causes a rather clear reduction of the magnetization at the wall, which is reflected by the absolute magnitude of the signal (see Fig. 8). Therefore, a thorough evaluation of the absolute signal strength—rather than relative quantities such as the slope s—may in principle provide more accurate information about ε. However, at present the knowledge of some of the experimental parameters is rather limited in accuracy and this prevents a safe evaluation of this kind. The Na number density has to be determined from the optical transmissivity of the sample, which is too low at the operating temperature to be measured accurately, so a rather uncertain extrapolation from lower temperatures is necessary. The tabulated vapor pressure [35] is not applicable, at least in the coated cell. We observed a considerably lower vapor density in this cell than in the uncoated one, even though the temperature was higher. We attribute this to the absorption of Na by the silicone layer. Related observations have been reported by other authors [36,37].

The comparison of the amplitudes measured with the coated and the uncoated cell—after rescaling the results to equal vapor densities and laser powers—nevertheless allows us to derive an improved estimate for ε. Even though this comparison is accurate only within a factor of ~ 2, it provides a more stringent boundary for ε. We find $\varepsilon<0.04$, which is fully compatible with the value of the order of 0.01 determined from the magnetic resonance line [32]. Note that such a relative comparison of amplitudes requires the knowledge of μ, in contrast to the evaluation of the line shape and the slope s. All theoretical curves in Figs. 6 and 8 were calculated with $1/\mu=56$ μm and $L=0.6$ μm. A different μ leaves the shape of the curves essentially unchanged but modifies not only their absolute magnitude but also their relative magnitude with respect to each other. For example, with increasing pump power μ increases and the curves move up and closer together, as the magnetization at the wall is driven closer to saturation.

V. CONCLUSIONS AND OUTLOOK

We have presented an experiment for the quantitative investigation of the spin relaxation of optically pumped atoms at a surface. The magnetization is sensed in the proximity of the surface by a laser beam that is reflected at the surface. The change of its polarization, which is induced by the anisotropy of the atomic vapor, is monitored. The combination of an optical and a magnetic resonance ensures a very high sensitivity, allowing the detection of less than 10^5 polarized atoms. The analysis of the data is based on the fact that the atoms are subject to a diffusive motion in an inert buffer gas. The interplay of diffusion, optical pumping, and wall relaxation results in the formation of an optically inhomogeneous layer, where the magnetization decreases toward the surface, its magnitude at the surface being determined by the extent of wall relaxation.

The theoretical analysis of the reflection at this inhomogeneous medium shows that the wall relaxation is reflected by the shape and strength of the optical line observed when the laser frequency is tuned across the atomic resonance. Strong wall relaxation causes a very clear modification of the line shape for angles of incidence immediately below the critical angle of total internal reflection, which can be utilized to deduce the depolarization probability ε per wall collision numerically. For a bare glass surface we find $\varepsilon \approx 0.5$. Measurements with a silicone-coated surface show that the wall relaxation is much smaller in this case ($\varepsilon<0.1$), but the exact value of ε is not accessible by this type of measurement, because the line shape depends only weakly on ε for small wall relaxation. Similarly, the dependence of the signal strength on the angle of incidence provides a useful measure of ε only for strong depolarization at the surface. A relative comparison of the signal amplitudes measured with the two surfaces indicates that the depolarization probability at the silicone layer is below 0.04. As we will discuss in detail in a

forthcoming paper, the magnetic-resonance line provides complementary information [32]. Essentially, the magnetic-resonance line is sensitive to ε in the region where the optical line is rather insensitive, and vice versa. Hence, both methods together represent a powerful tool for the study of wall relaxation over a wide range of ε.

The value $\varepsilon = 0.5$ found for the glass surface is lower than one might expect from the adsorption energy of 0.71 eV that has been reported for Na on Pyrex glass in the literature [38]. From this energy a rather long average dwell time on the surface of the order of 1 μs follows, which should lead to an efficient depolarization. However, one should first of all be aware that the surface used in the experiment is not well defined and its exact composition is not known. Further measurements including several samples of the same kind are necessary to clarify the reproducibility of the results and the possible presence of contaminants. Measurements of the wall relaxation of spin polarized Xe nuclei reported by Zeng *et al.* showed large fluctuations for bare glass surfaces [39]. On the other hand, a long average dwell time on the surface does not necessarily imply that ε is close to unity. If a considerable fraction of the wall collisions are collisions where the atom does not stick to the surface but immediately bounces back to the gas phase, the average depolarization should be clearly below unity although the average dwell time still might be very long. In other words, in this case the study of the depolarization probability ε provides access to the sticking probability at the surface, which is an important quantity for adsorption kinetics [40].

As discussed in this paper, the description of the basic optical line shape as Lorentzian represents an oversimplification and this introduces a considerable uncertainty into the deduction of the depolarization probability. Therefore, a further development of the method should include a more elaborate treatment taking the hyperfine structure and the Doppler effect into account. Furthermore, the usage of separate lasers for pumping and probing would allow us to keep the frequency of the pump beam fixed. This would simplify the evaluation, as it eliminates the modification of the atomic medium that results from the frequency tuning of the pump beam.

The method bears the potential to be applied to a wider class of surfaces, including different coatings and also crystalline surfaces, such as, e.g., LiF. It is, of course, highly desirable to improve the surface preparation, as well-defined surfaces are indispensable for the reproducibility of the results and for their interpretation in terms of surface properties. An application of the method to various surfaces, preferably in a vacuum chamber offering strongly improved possibilities of preparation and control, is very much facilitated by the fact that only the illuminated area of the surface is probed, which can be rather small. This is an important advantage as compared with arrangements, in which information about wall relaxation is deduced from the magnetization in the volume of the atomic vapor, in which case all surrounding surfaces contribute.

ACKNOWLEDGMENTS

This research was supported by the Schweizerischer Nationalfonds and a ''human capital and mobility'' grant from Bundesamt für Bildung and Wissenschaft (Contract No. 93.0231). Assistance from Tilo Blasberg is gratefully acknowledged.

[1] S. LeBoiteux, P. Simoneau, D. Bloch, and M. Ducloy, J. Phys. B. **20**, L149 (1987).
[2] P. Simoneau, S. LeBoiteaux, C. B. DeAraujo, D. Bloch, J. R. Leite, and M. Ducloy, Opt. Commun. **59**, 103 (1986).
[3] A. M. Akul'shin, V. L. Velichanskii, A. I. Zherdev, A. S. Zibrov, V. I. Malakhova, V. V. Nikitin, V. A. Sautenkov, and G. G. Kharisov, Kvant. Elektron. (Moscow) **16**, 631 (1989) [Sov. J. Quantum Electron. **19**, 416 (1989)].
[4] A. Weis, V. A. Sautenkov, and T. W. Hänsch, Phys. Rev. A **45**, 7991 (1992).
[5] M. Oria, M. Chevrollier, D. Bloch, M. Fichet, and M. Ducloy, Europhys. Lett. **14**, 527 (1991).
[6] M. F. H. Schuurmans, J. Phys. **37**, 469 (1976).
[7] A. L. J. Burgmans and J. P. Woerdman, J. Phys. **37**, 677 (1976).
[8] G. Nienhuis, F. Schuller, and M. Ducloy, Phys. Rev. A **38**, 5197 (1988).
[9] M. Ducloy, Opt. Commun. **99**, 336 (1993).
[10] M. Ducloy and M. Fichet, J. Phys. (France) II **1**, 1429 (1991).
[11] D. Suter, J. Äbersold, and J. Mlynek, Opt. Commun. **84**, 269 (1991).
[12] S. Grafström, T. Blasberg, and D. Suter, J. Opt. Soc. Am. B **13**, 3 (1996).
[13] S. Grafström and D. Suter, Opt. Lett. **20**, 2134 (1995).
[14] W. Happer, Rev. Mod. Phys. **44**, 169 (1972).
[15] M. A. Bouchiat and J. Brossel, Phys. Rev. **147**, 41 (1966).
[16] D. R. Swenson and L. W. Anderson, Nucl. Instrum. Methods B **12**, 157 (1985).
[17] C. D. P. Levy and P. W. Schmor, J. Appl. Phys. **63**, 4819 (1988).
[18] D. R. Swenson and L. W. Anderson, Nucl. Instrum. Methods B **29**, 627 (1988).
[19] M. Tanaka, T. Ohshima, K. Katori, M. Fujiwara, T. Itahashi, H. Ogata, and M. Kondo, Phys. Rev. A **41**, 1496 (1990).
[20] Z. Wu, W. Happer, M. Kitano, and J. Daniels, Phys. Rev. A **42**, 2774 (1990).
[21] R. Butscher, G. Wäckerle, and M. Mehring, J. Chem. Phys. **100**, 6923 (1994).
[22] H. D. Ebinger, M. Detje, H. J. Jänsch, C. Polenz, B. Polivka, W. Preyss, V. Saier, R. Veith, and D. Fick, Surf. Sci. **331-333**, 759 (1995).
[23] H. Klepel and D. Suter, Opt. Commun. **90**, 46 (1992).
[24] M. Allegrini, P. Bicchi, L. Moi, and P. Savino, Opt. Commun. **32**, 396 (1980).
[25] D. Suter, Opt. Commun. **86**, 381 (1991). The expression given in this reference has been modified to apply to a time dependence $\exp(-i\omega t)$ as used in Ref. [8].
[26] M. Born and E. Wolf, *Principles of Optics*, 5th ed. (Pergamon, Oxford, 1975).

[27] The integral given in Ref. [8] was transformed by integration by parts, assuming an arbitrarily small damping of the exciting wave.
[28] *The Solid-Gas Interface*, edited by E. Alison Flood (Marcel Dekker, New York, 1967), Vol 2.
[29] In Ref. [13] m_∞ was subsumed in $v_{\rm hom}$, whereas here we keep it as a separate factor.
[30] *Landolt-Börnstein Zahlenwerte und Funktionen aus Physik, Chemie, Astronomie, Geophysik und Technik*, 6th ed., edited by H. Borchers *et al.* (Springer, Berlin, 1969), Vol. II, Sec. 5a, p. 536.
[31] D. Suter and J. Mlynek, Phys. Rev. A **43**, 6124 (1991).
[32] S. Grafström and D. Suter, Z. Phys. D (to be published).
[33] The damping also contains a power-dependent contribution due to radiation trapping, which we here may subsume in P.
[34] F. O. Goodman and H. Y. Wachman, *Dynamics of Gas-surface Scattering* (Academic, New York, 1976).
[35] *Selected Values of the Thermodynamic Properties of the Elements*, edited by R. Hultgren *et al.* (American Society for Metals, Metals Park, OH, 1973).
[36] A. Gozzini, F. Mango, J. H. Xu, G. Alzetta, F. Maccarrone, and R. A. Bernheim, Nuovo Cimento D **15**, 709 (1993).
[37] M. Meucci, E. Mariotti, P. Bicchi, C. Marinelli, and L. Moi, Europhys. Lett. **25**, 639 (1994).
[38] S. Gozzini, G. Nienhuis, E. Mariotti, G. Paffuti, C. Gabbanini, and L. Moi, Opt. Commun. **88**, 341 (1992).
[39] X. Zeng, E. Miron, W. A. van Wijngaarden, D. Schreiber, and W. Happer, Phys. Lett. **96A**, 191 (1983).
[40] A. Zangwill, *Physics at Surfaces* (Cambridge University Press, Cambridge, 1988).